

# Fault-zone damage promotes pulse-like rupture and back-propagating fronts via quasi-static effects

B. Idini\*<sup>1</sup> and J.-P. Ampuero<sup>2</sup>

<sup>1</sup>Seismological Laboratory, California Institute of Technology, 1200 E. California Blvd., Pasadena, CA 91775, USA

<sup>2</sup>Université Côte d'Azur, IRD, CNRS, Observatoire de la Côte d'Azur, Géoazur, 250 Rue Albert Einstein, 06560 Valbonne, France

## Key Points:

- Highly damaged fault zones promote pulse-like ruptures even without the dynamic effects of reflected waves.
- Slip complexity induced by fault damage involves multiple back-propagating rupture fronts.
- A new mechanism for Rapid-Tremor-Reversals observed during Episodic Tremor and Slip.

## Keywords

rupture dynamics · slow earthquakes · fault zone · damaged zone · rapid-tremor-reversals

---

Corresponding author: Benjamin Idini, [bidiniza@caltech.edu](mailto:bidiniza@caltech.edu)

**Abstract**

Damage zones are ubiquitous components of faults that may affect earthquake rupture. Simulations show that pulse-like rupture can be induced by the dynamic effect of waves reflected by sharp fault zone boundaries. Here we show that pulses can appear in a highly damaged fault zone even in the absence of reflected waves. We use quasi-static scaling arguments and quasi-dynamic earthquake cycle simulations to show that a crack turns into a pulse after the rupture has grown larger than the fault zone thickness. Accompanying the pulses, we find complex rupture patterns involving back-propagating fronts that emerge from the primary rupture front. Our model provides a mechanism for back-propagating fronts recently observed during large earthquakes. Moreover, we find that slow-slip simulations in a highly-compliant fault zone also produce back-propagating fronts, suggesting a new mechanism for the rapid-tremor-reversals observed in Cascadia and Japan.

**Plain Language Summary**

Damage zones are zones of fractured rock that surround faults and can influence how earthquakes propagate. Previous computer models show that damage zones promote an inchworm-like (rather than zipper-like) pattern of earthquake propagation, known as pulses. This finding has been previously attributed to the effect of seismic waves reflected at the boundaries of the damage zone. Here, we show that pulses are generated in highly-fractured damage zones independently of the reflection of seismic waves. We reach this conclusion by scaling arguments confirmed by numerical simulations of sequences of earthquakes in which we ignore the reflection of seismic waves. Moreover, our models produce an unexpected pattern of earthquake propagation: secondary rupture fronts emerge from the primary rupture front and propagate in the opposite direction. Similar back-propagating fronts have been previously observed during slow earthquakes in subduction zones and more recently during large earthquakes. Our work reveals a possible connection between an observable structural feature of faults and complicated patterns of earthquake propagation.

**1 Introduction**

Pulse-like rupture (hereafter referred to as pulses) is a common mode of earthquake propagation in which the duration of slip at each point of the fault, known as the rise-time, is short compared to the total rupture duration (Heaton, 1990). Pulses play a prominent role in the theory of earthquake mechanics: they can radically affect the earthquake energy balance (Nielsen & Madariaga, 2003), reduce the apparent strength of faults (Noda et al., 2009), enhance the spatial heterogeneity of earthquake slip and stress (Aagaard & Heaton, 2008), and promote complexity of seismicity manifested by a broad range of event magnitudes (Cochard & Madariaga, 1996). Yet their origin is not completely established. Several mechanisms of pulse generation have been proposed, involving healing fronts emerging from features of the friction law (Cochard & Madariaga, 1996; G. Perrin et al., 1995), from early arrest of one dimension of rupture (Day, 1982; Johnson, 1990), from fault heterogeneities (Beroza & Mikumo, 1996; Day et al., 1998) or from waves reflected in a low-velocity fault damage zone (Huang & Ampuero, 2011). The present work focuses on the generation of pulses by damaged zones.

Faults are usually embedded in a damaged zone (Fig. 1a) characterized in field observations by distributed fractures and micro-cracks (Chester & Logan, 1986; Mitchell & Faulkner, 2009; Savage & Brodsky, 2011) and in seismological and geodetic observations by reduced wave speeds or elastic modulus relative to the host rock (Y.-G. Li et al., 1990, 2002; Ben-Zion et al., 2003; Peng et al., 2003; M. Lewis et al., 2005; Y.-G. Li et al., 2006; H. Li et al., 2007; Mizuno et al., 2008; Cochran et al., 2009; M. A. Lewis & Ben-Zion, 2010; Yang & Zhu, 2010; Yang et al., 2011). Seismic imaging methods resolve fault zones of strike-slip faults as flower-structures with depth-varying thickness and dam-

age (Ben-Zion et al., 2003; Finzi et al., 2009). Hereafter, we refer to these structures as low-velocity fault zones (LVFZ).

Dynamic rupture simulations show that the presence of a LVFZ can induce complex rupture patterns: pulses promoted by healing fronts mediated by reflected waves, oscillations of slip-rate and rupture speed, and supershear rupture at low background stress (Harris & Day, 1997; Huang & Ampuero, 2011; Huang et al., 2014, 2016). Recent earthquake cycle simulations show that the generation of pulses by a LVFZ is persistent across multiple earthquake cycles, both in fully-dynamic (Thakur et al., 2020) and quasi-dynamic simulations (Idini & Ampuero, 2017). The mechanism of pulse generation by a LVFZ has been previously attributed to the dynamic effect of waves reflected at the boundary of the LVFZ, which tend to unload the fault and promote slip arrest (Huang & Ampuero, 2011; Thakur et al., 2020). However, LVFZ quasi-dynamic simulations do not include these reflected waves. Here, we explain how pulses can be promoted in LVFZs by a quasi-static mechanism.

The present work is further motivated by recent evidence of complex rupture patterns in earthquakes and tectonic tremors, in particular back-propagating fronts. While the inherent complexity of large earthquakes is abundantly highlighted by modern seismological observations (Meng et al., 2012; Ross et al., 2019), reports of secondary rupture fronts propagating in the direction opposite to the main front (i.e., towards the hypocenter) are becoming increasingly clear and robust (Beroza & Spudich, 1988; Meng et al., 2011; Uchide et al., 2013; Hicks et al., 2020; Vallée et al., 2020). Back-propagating fronts have also been identified during slow slip events (SSE) in Cascadia and Japan, appearing as tremor swarms known as Rapid Tremor Reversals (RTR) which migrate at fast speed in the direction opposite to the propagation of the large-scale slow slip (Houston et al., 2011).

Here, we show that pulses can be generated by a highly-damaged LVFZ, even without the dynamic effects of reflected waves. We follow two complementary approaches: static rupture scaling arguments (Section 2) and quasi-dynamic earthquake cycle simulations (Section 3). Our simulations also reveal that the quasi-static effects of a highly-damaged LVFZ are sufficient to generate back-propagating fronts.

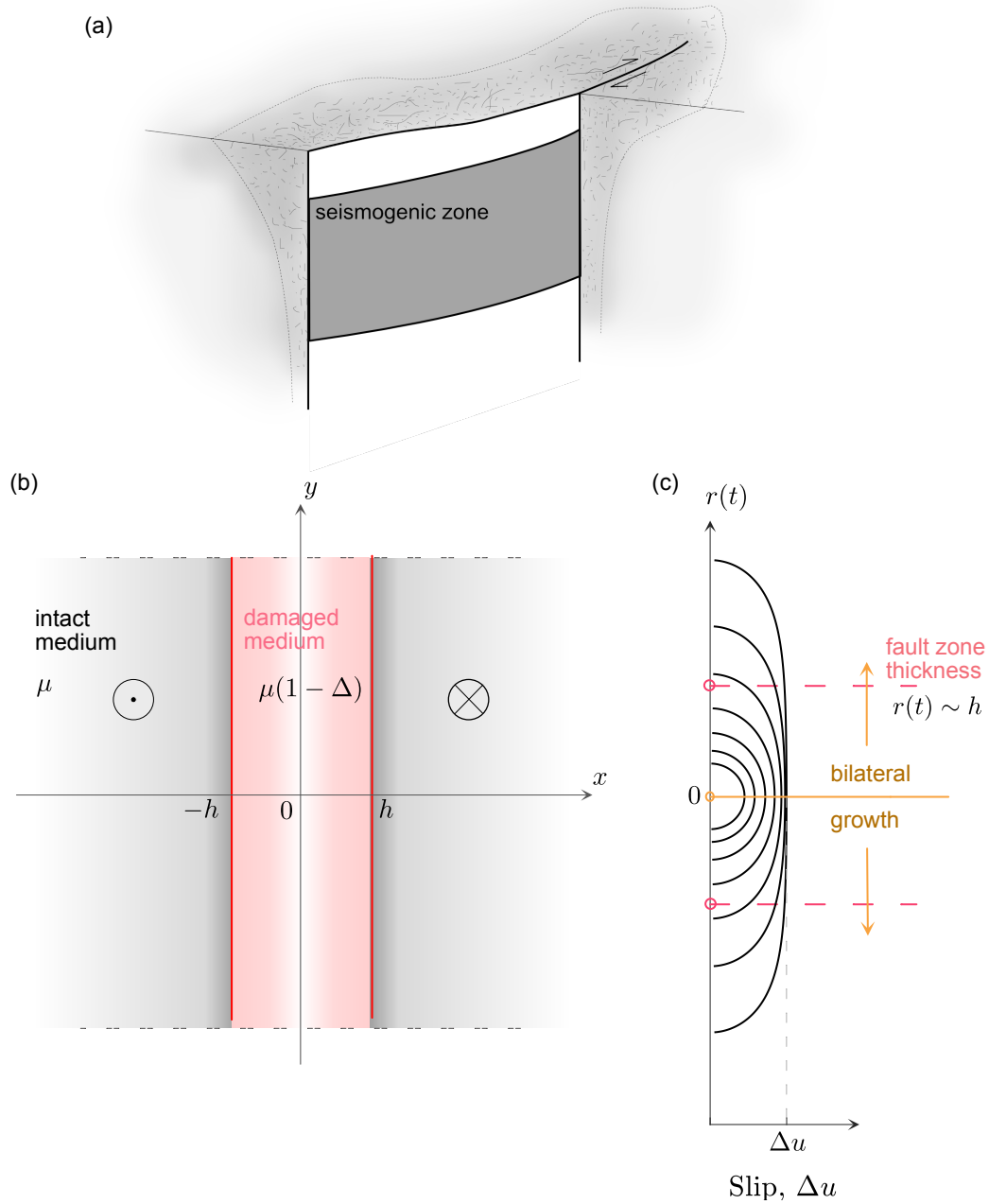
## 2 Scaling arguments for quasi-static pulse generation

We consider a simple, tabular LVFZ model defined by a finite fault of length  $L$  bisecting a homogeneous low-rigidity layer, the damage zone, embedded in an intact medium (Fig. 1). The LVFZ is specified by its half-thickness  $h$  and its damage level  $\Delta$  defined by:

$$\mu_d = (1 - \Delta)\mu \quad (1)$$

where  $\mu_d$  and  $\mu$  are the shear moduli of the LVFZ and intact medium, respectively. We consider anti-plane deformation. The model converges to two different homogeneous end-member models, depending on the fault zone thickness. When  $h/L$  is very small, the model approaches a homogeneous intact medium with shear modulus  $\mu$ . When  $h/L$  is very large, the model tends to a homogeneous damaged medium with shear modulus  $(1 - \Delta)\mu$ .

Key effects of a LVFZ on rupture propagation are highlighted by analyzing the limiting case of a highly damaged fault zone ( $\Delta \rightarrow 1$ ), which is asymptotically equivalent to the case of a rigid medium surrounding an elastic fault zone considered by (Horowitz & Ruina, 1989). We consider a rupture growing quasi-statically with prescribed uniform stress drop  $\Delta\tau$  and increasing rupture half-length  $r(t)$ . The fault-zone thickness  $h$  is fixed and, for illustrative purposes, we set  $\Delta = 0.99$ . The resulting slip profiles (Fig. 1c) are computed by solving numerically a static problem in which we account for static stress interactions modified by the presence of the damaged layer, as described in Text S2. The shape of the slip profile is indicative of the style of rupture: crack-like ruptures show an



108

109 **Figure 1.** (a) Schematic representation of a fault zone. (b) Conceptualization of a fault zone  
 110 as a simple tabular Low Velocity Fault Zone (LVFZ) model. The damaged and intact media have  
 111 constant shear modulus,  $(1 - \Delta)\mu$  and  $\mu$ , respectively. (c) Quasi-static rupture growth with uni-  
 112 form stress drop in a LVFZ, showing a transition from crack-like (elliptical) to pulse-like (flat)  
 113 slip profiles when the rupture length exceeds the LVFZ thickness. The static slip profiles are  
 114 computed numerically for  $\Delta = 0.99$  by the method described in Text S2.

124 elliptical slip profile whereas (steady-state) pulses have a flat slip profile (Gabriel et al.,  
 125 2012). While the rupture is small ( $r(t) \ll h$ ), it only interacts with the damaged zone  
 126 and therefore has a crack-like slip profile, as in a uniformly damaged infinite medium.  
 127 Its slip grows proportional to rupture length as  $\Delta u(t) \sim \frac{\Delta\tau}{2\mu(1-\Delta)}r(t)$ . As the rupture  
 128 grows large ( $r(t) \gg h$ ), it interacts with a thin elastic slab of thickness  $h$  and devel-  
 129 ops a pulse-like slip profile. Its slip reaches a value independent of rupture length,  $\Delta u \sim$   
 130  $\frac{\Delta\tau}{\mu(1-\Delta)}h$ , as expected in a thin slab problem. Connecting these two rupture stages to-  
 131 gether, a growing rupture with constant stress drop in a highly-damaged LVFZ will initi-  
 132 ate as a crack-like rupture and later transition into a pulse. The transition is charac-  
 133 terized by saturation of slip caused by the LVFZ once the rupture grows larger than  $2h$ .

134 The above picture of crack-to-pulse transition provides insight into what controls  
 135 rise-time in a damaged fault zone in the absence of wave reflection effects. The rise-time  
 136 at the hypocenter is the time required for the appearance of a healing front. This time  
 137 corresponds kinematically to the emergence of pulses, which is approximately the time  
 138 required for the size of the initial crack to grow up to  $r(t) = h$ . Assuming a constant  
 139 rupture speed  $v_r$ , the size of the rupture is  $r(t) \sim v_r t$ , hence the rise time at the hypocen-  
 140 ter roughly follows:

$$t \sim \frac{h}{v_r} \quad (2)$$

141 This estimation of rise-time is valid at other locations beyond the hypocenter assuming  
 142 that the propagation speed of the healing front is close to the rupture speed. Because  
 143 rise-time can be shorter away from the hypocenter (Huang & Ampuero, 2011), Eq. (2)  
 144 should be taken as an upper bound. The resulting upper bound for the pulse width, de-  
 145 fined as the distance between the position of the rupture front and the healing front, is:

$$l \sim v_r t \sim h \quad (3)$$

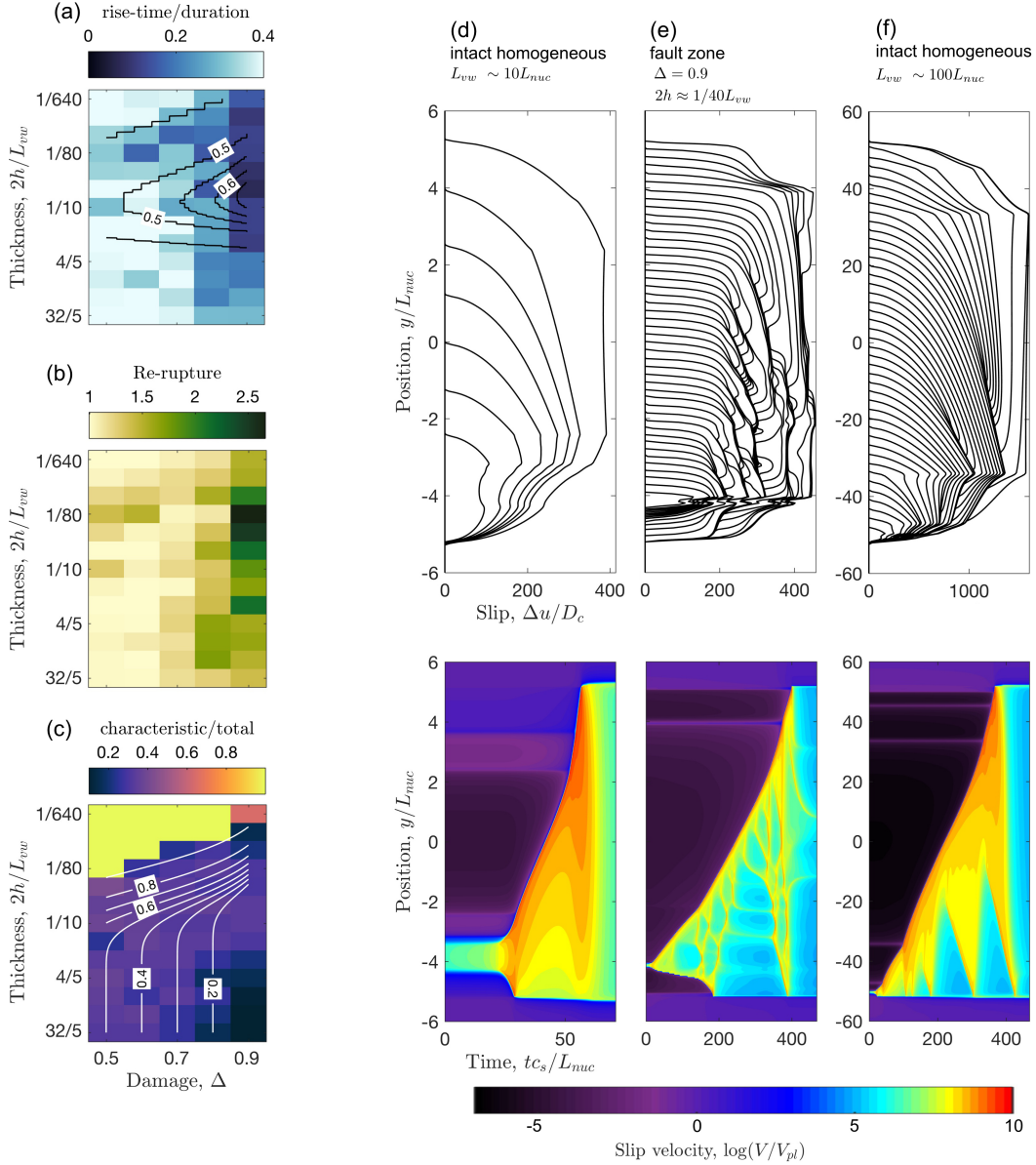
146 The foregoing simplified analysis predicts the emergence of pulses from static effects alone,  
 147 independently of the presence of reflected waves in the LVFZ.

### 148 **3 Pulses and back-propagating fronts in quasi-dynamic multi-cycle mod-** 149 **els**

150 We conduct quasi-dynamic earthquake cycle simulations under rate-and-state fric-  
 151 tion (Text S1 for methods), covering a wide range of values of LVFZ thickness and dam-  
 152 age. Our simulations do not include dynamical effects from reflected waves. Each simu-  
 153 lation produces a history of seismic activity, including earthquakes with multiple sizes  
 154 (Fig. S1). The largest earthquakes in one simulation span the whole seismogenic length  
 155  $L_{vw}$  (Fig. S2) and are labeled as characteristic events. In a given fault model, charac-  
 156 teristic events have the same magnitude but may show different rupture patterns. We  
 157 define an earthquake cycle as the period between two characteristic events. In some fault  
 158 models, simulations show a variable duration of the earthquake cycle. We only consider  
 159 results in characteristic events after a spin-up period of several initial cycles, avoiding  
 160 a dependence of our results on the arbitrarily-prescribed initial conditions.

177 Complex slip patterns appear in characteristic events when damage is high ( $\Delta >$   
 178  $0.7$ ) and the fault zone is thin compared to the length of the seismogenic zone ( $2h <$   
 179  $L_{vw}$ ). Two signatures characterize the slip complexity: the promotion of pulses (Fig. 2a)  
 180 and the re-rupture of previously healed fault segments during the same event (Fig. 2b,e).

181 Pulses are defined here by a drastic reduction of slip rate ( $V < 1$  cm/s) at a short  
 182 distance behind the rupture front, leading to a short rise-time. We observe a systematic  
 183 reduction of the average rise-time over a wide range of LVFZ thickness and high dam-  
 184 age values (Fig. 2a). Short rise-times occur roughly within the range of LVFZ param-  
 185 eters that produce flat slip profiles in the static rupture models computed in Section 2



161

162 **Figure 2.** Properties of ruptures and seismicity in fault-zone models after multiple earthquake cycle  
 163 cycles and spatiotemporal evolution of slip and slip velocity in the characteristic event of earth-  
 164 quake cycle models. (a) Average rise-time normalized by the total rupture duration, (b) average  
 165 number of rupture fronts ( $V > 1$  cm/s) during an event, and (c) number of characteristic events  
 166 over the total number of events as a function of damage level  $\Delta$  and fault-zone thickness  $2h$  nor-  
 167 malized by the size of the velocity-weakening fault segment  $L_{vw}$ . The rise-time is defined here  
 168 as the duration of slip rate exceeding 1 cm/s. Black contour lines in (a) are a semi-analytical  
 169 prediction of the flatness of the slip profile in a constant stress drop model (Text S2). The slip  
 170 profiles are obtained with the same method used in Fig. 1c. Flatness is the fraction of the fault  
 171 length where slip is roughly constant, at most 20% lower than the maximum slip in the slip pro-  
 172 file. The white contours in (c) show the estimated reduction of the nucleation length due to the  
 173 LVFZ (contours of  $L_{nuc}$  in LVFZ normalized by its value in a homogeneous intact medium). (d)  
 174 Spatiotemporal evolution of slip and slip velocity in the characteristic event of an intact homo-  
 175 geneous medium, (e) a LVFZ with  $\Delta = 0.9$  and  $2h \approx L_{vw}/40$ , and (f) an intact homogeneous  
 176 medium with ten times smaller nucleation length than (d).

186 (Fig. 2a), consistent with the kinematic implications we drew from the static crack anal-  
 187 ysis.

188 The re-rupture of previously healed fault segments (Fig. 2b) is characterized by the  
 189 emergence of secondary fronts propagating in the opposite direction to the main rupture  
 190 front (Fig. 2e and Fig. S3). These back-propagating fronts have a short rise-time and  
 191 can re-rupture multiple times the same fault segment. Models with seismogenic zones  
 192 that are much larger than the nucleation size ( $L_{vw} \gg L_{nuc}$ ; Text S1) promote back-  
 193 propagating fronts without requiring a LVFZ, but their rise-time is longer and their num-  
 194 ber of re-ruptures is small (Fig. 2f with  $L_{vw} \sim 100L_{nuc}$ ).

195 In addition to characteristic events with complex slip patterns, events comprising  
 196 a wide range of sizes develop in thick and highly damaged fault zones (Fig. 2c), where  
 197 small events partially break the seismogenic zone from the edges (Fig. S1). Small, non-  
 198 characteristic events are known to emerge in rate-and-state friction models in homoge-  
 199 neous media with seismogenic zones much larger than their nucleation length  $L_{nuc}$  (Cattania,  
 200 2019; Barbot, 2019). The nucleation length is the smallest size of a slip patch that can  
 201 accelerate to instability (Rubin & Ampuero, 2005). In a homogeneous medium it is pro-  
 202 portional to the shear modulus, and in a damaged zone to a reduced, effective shear mod-  
 203 ulus that depends on  $h$  and  $\Delta$  (Text S1). The LVFZ thickness and damage values pro-  
 204 moting variable event magnitudes in our models are well explained by the increase in the  
 205  $L_{vw}/L_{nuc}$  ratio due to the reduction in  $L_{nuc}$  induced by the LVFZ (Fig. 2c). The small-  
 206 est nucleation length is achieved in models with  $\Delta = 0.9$  and  $2h > L_{vw}$ , which have  
 207  $L_{vw} \sim 100L_{nuc}$ .

214 The rupture speed in our homogeneous medium model (Fig. 2d) corresponds to  $V_{rup} \sim$   
 215 1 km/s, a typical value in seismological observations. In contrast, a highly-damaged fault  
 216 zone promotes a reduction in the rupture speed  $V_{rup}^d/V_{rup} \propto (1-\Delta)$ , compatible with  
 217 theoretical quasi-static predictions of rupture speed (Ampuero & Rubin, 2008) but slower  
 218 than most seismological observations. The non-dimensional units in Fig. 2 can be con-  
 219 verted into real scales depending on the assumed value of the characteristic slip distance  
 220 of rate-and-state friction,  $D_c$ ; examples of dimensional scales are given in Table S1 for  
 221  $D_c = 2$  mm.

## 222 4 Discussion

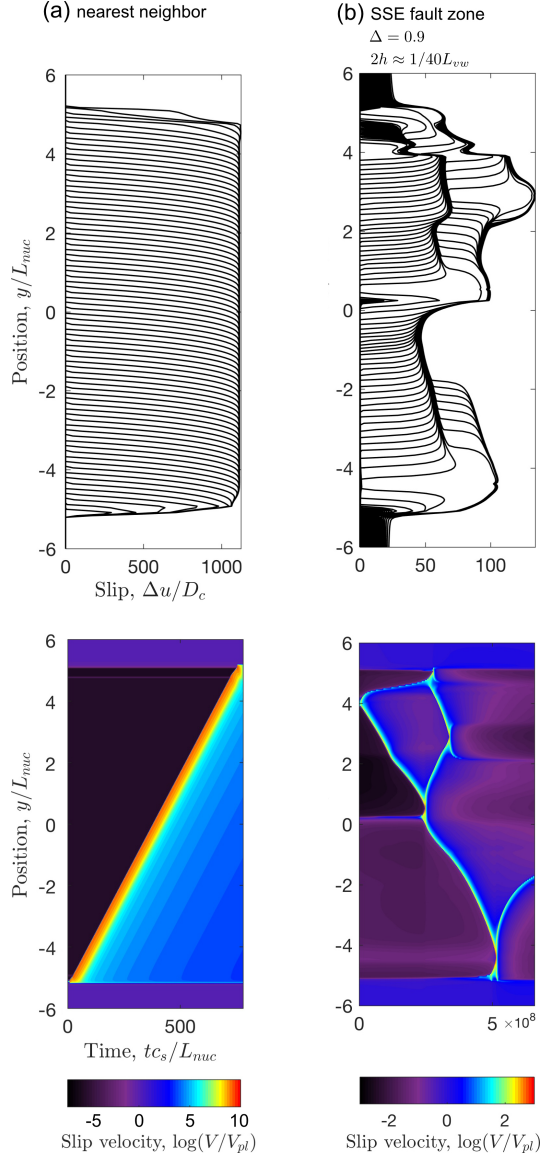
### 223 4.1 Short-range stress transfer and the origin of pulses in a LVFZ

224 Models with nearest-neighbour stress transfer, such as the Burridge-Knopoff (BK)  
 225 model (Burridge & Knopoff, 1967), have been often used as a mechanical analog to earth-  
 226 quake rupture and are capable of promoting pulses in the continuum limit (Erickson et  
 227 al., 2011; Brener et al., 2018). In a BK model, a chain of sliders connected by springs  
 228 is loaded by a uniform displacement applied to a loading spring (Burridge & Knopoff,  
 229 1967). In a uniform stress drop rupture, the BK model produces the flat static slip pro-  
 230 file characteristic of pulses when the loading stiffness is much higher than the static stress  
 231 transfer due to the relative motion of sliders (Text S3). Under our current model param-  
 232 eters (Table S2), ruptures propagate as pulses both in a nearest-neighbour model (Fig. 3a)  
 233 and in a fault-zone model with large damage,  $\Delta = 0.9$  (Fig. 2e). Here we show that the  
 234 emergence of pulses in a LVFZ can be related to stress interactions approaching the nearest-  
 235 neighbour regime across a wide range of slip wavelengths.

246 The static stress transfer in a fault-zone model due to spatially-harmonic slip with  
 247 wavelength  $k$  and unit amplitude is (Text S2, Fig. S4):

$$\mathcal{K}(k) = \frac{1}{2}\mu(1 - \Delta)|k| \coth(h|k| + \operatorname{atanh}(1 - \Delta)) \quad (4)$$

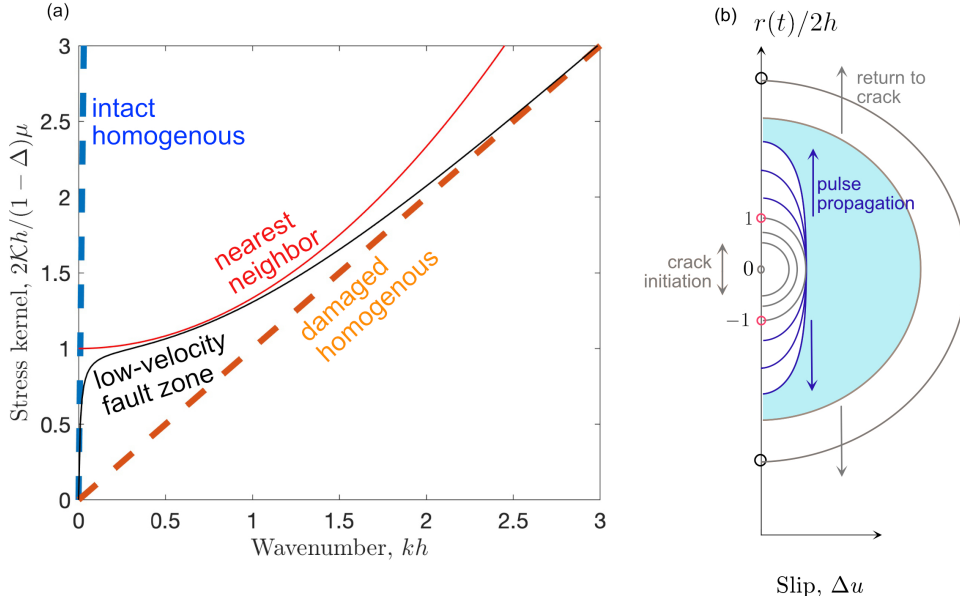




208

209 **Figure 3.** Spatiotemporal evolution of slip and slip rate in the characteristic event of earth-  
 210 quake cycle models assuming (a) a nearest-neighbor model with  $\Delta = 0.99$  and  $2h = L_{vw}/25$  and  
 211 (b) a slow-slip model in a LVFZ model with  $\Delta = 0.9$  and  $2h \approx L_{vw}/40$  and a modified friction  
 212 law with velocity-strengthening at high velocities. Axes are normalized following the convention  
 213 in Fig. 2.





236

237 **Figure 4.** Nearest-neighbor stress transfer and promotion of slip complexity. (a) The static  
 238 stress transfer kernel of a LVFZ (Eq. 4) with  $\Delta = 0.99$  (black) in Fourier domain, as a func-  
 239 tion of the normalized wavenumber  $kh$  of slip, and its nearest-neighbor approximation (red)  
 240 (Text S3). Also shown are the asymptotic limits of a homogeneous intact medium (blue dashed)  
 241 ( $\mathcal{K} = \mu|k|/2$ ) and homogeneous damaged medium (orange dashed) ( $\mathcal{K} = \mu_d|k|/2$ ). The exagger-  
 242 ated level of damage  $\Delta = 0.99$  represents the asymptotic limit of a LVFZ as damage increases.  
 243 (b) Conceptual interpretation of the emergence of secondary pulses. Re-rupturing is necessary  
 244 to fill the slip deficit (cyan) between a pulse at intermediate rupture length ( $r(t) > 2h$ , purple  
 245 curves) and a crack appearing at much larger lengths ( $r(t) \gg 2h$ , gray curves).

Asymptotic analysis (Fig. 4a, Text S3) shows that at low  $k$  the stress transfer in a LVFZ tends to that of an intact homogeneous medium, whereas at high  $k$  it tends to that of a damaged homogeneous medium. In an intermediate range of wavelengths, the stress transfer is approximately nearest-neighbour. As  $\Delta$  increases, the relative bandwidth of the nearest-neighbour regime broadens (Fig. S8), and the short rise-time observed in the nearest-neighbor model (Fig. 3a) appears in the LVFZ model as well. In other words, increasing the LVFZ damage level extends the range of slip length scales where pulses can exist. When  $h$  is small ( $h \ll \sqrt{3}L_{vw}$ ), a LVFZ model within the nearest-neighbour regime produces uniform stress drop ruptures with a slip profile that is flat and has an average slip  $\approx 2h\Delta\tau/(1 - \Delta)\mu$  (Text S3).

The limiting case where  $\Delta \rightarrow 1$ , analyzed in Section 2, represents an elastic layer of thickness  $2h$  bounded by an infinitely rigid medium (Horowitz & Ruina, 1989). Stress interactions in that case are nearest-neighbour at wavelengths larger than  $\sim 2\pi h$  (Fig. S8). Such model is completely nearest-neighbour if the process zone size, the smallest characteristic length scale of slip, is larger than  $\sim 2\pi h$ .

## 4.2 Origin of back-propagating fronts

Highlighted in our work as a manifestation of rupture complexity, back-propagating fronts owe part of their relevance to recent earthquake observations. A recent report from a M7.1 oceanic transform earthquake features a “boomerang earthquake” slip pattern (Hicks et al., 2020) that resembles the structure of back-propagating fronts shown in our models. Seismic observations indicate that LVFZs extend throughout the seismogenic zone in oceanic transform faults (Roland et al., 2012), enhancing the relevance of our model to explain the “boomerang earthquake” slip pattern. In a different tectonic setting, a back-propagating front appears during a recently reported M8 intermediate-depth earthquake (Vallée et al., 2020). Both observations are independently supported by teleseismic back-projection imaging and finite source inversion, suggesting the ubiquity of back-propagating fronts to different tectonic environments.

The static solutions introduced in Section 2 provide insight on the origin of multiple back-propagating fronts. Relying on an idealized situation where the only deformable medium is within the LVFZ, we showed the emergence of a transition from a crack into a pulse when the rupture size exceeds  $2h$ . In reality the medium outside the LVFZ is deformable as well. As the rupture continues growing to sizes much larger than  $2h$ , stress increasingly transfers through the outer medium. Eventually, the influence of the LVFZ becomes irrelevant to the propagation of the rupture. At this point, the static analysis predicts a second, reverse transition from pulse-like behavior to the crack-like behavior of an intact homogeneous medium (Fig. 4b). Beyond this transition, slip increases in regions that were previously healed. Therefore, slip reactivation is required there, leading to secondary rupture fronts.

We expect re-ruptures to initiate where stresses are the highest, which is near the primary rupture front, thus the ensuing secondary rupture fronts have to propagate backwards. Furthermore, because these secondary ruptures start small, they need to go through a pulse-like phase. In summary, in the presence of a LVFZ, back-propagating pulses are necessary to complete the slip budget of a very large rupture, filling the slip gap between intermediate-size pulses and large-size cracks.

## 4.3 A mechanism for Rapid Tremor Reversals

While observations of back-propagating fronts during earthquakes are challenging and still incipient, slow slip and tremor phenomena offer a unique and systematic opportunity to observe complex slip patterns in slow motion. The back-propagating fronts identified in Fig. 2e suggest that a highly-compliant LVFZ can provide a mechanism for

297 Rapid Tremor Reversals (RTRs) observed in Cascadia and Japan during slow-slip events  
 298 (Houston et al., 2011). Seismological observations suggest that subduction megathrusts  
 299 are surrounded by low-velocity zones (Nedimović et al., 2003; Audet & Schaeffer, 2018)  
 300 that are several kilometers thick near the region where tremor activity concentrates (Calvert  
 301 et al., 2020). Instead of damaged rock, low-velocity zones in subduction zones mostly  
 302 relate to layers of subducted material containing pressurized fluids. Previous models of  
 303 RTR rely on frictional heterogeneities (Luo & Ampuero, 2017; Luo & Liu, 2019), pore  
 304 fluid pressure waves (Cruz-Atienza et al., 2018), or external transient forcings such as  
 305 tides (Hawthorne & Rubin, 2013b). Our models show RTR-like patterns emerging from  
 306 a different mechanism: the quasi-static stress transfer of a LVFZ. Due to the ubiquity  
 307 of LVFZ to both regular earthquakes and slow slip events, our model supports the idea  
 308 that detailed observations of slow slip phenomena contribute to understand earthquakes  
 309 in general (Michel et al., 2019).

310 (Nedimović et al., 2003; Audet & Schaeffer, 2018) (Calvert et al., 2020).

311 Our simulations show that back-propagating fronts also occur in slow slip models  
 312 with a LVFZ (Fig. 3b). Introducing strengthening at high slip rate is a known approach  
 313 to model slow-slip events (Hawthorne & Rubin, 2013a). We added a linear velocity-strengthening  
 314 term into the friction law (i.e., the fault strengthens proportionally to  $V$ ), which is stronger  
 315 than the logarithmic strengthening term of the conventional rate-and-state friction (Text  
 316 S1). We chose a velocity-strengthening coefficient  $10^6$  times larger than the radiation damp-  
 317 ing coefficient. Our results indicate that back-propagating fronts emerge during slow-  
 318 slip events in a LVFZ model with the modified friction, although they are less vigorous  
 319 than those observed in our fast-rupture results (Fig. 3). Slow-slip events only show pulse-  
 320 like behavior and back-propagating fronts in the presence of a LVFZ (Fig. S5). As slow-  
 321 slip models are insensitive to dynamical effects, our results confirm that back-propagating  
 322 fronts emerge from quasi-static LVFZ effects alone. The SSE propagation speed in our  
 323 model is  $\sim 5$  m/day, about 1000 times lower than SSE propagation speeds observed in  
 324 Cascadia, which range from 7 to 15 km/day (Houston et al., 2011). Further work is re-  
 325 quired to examine how low-velocity zones quantitatively affect tremor migration patterns  
 326 in more detailed slow-slip models.

327 The damage level observed in strike-slip faults ranges from 0.45 to 0.85 and the fault  
 328 zone thickness from 80 to 1500 m, with typical values  $\Delta \sim 0.65$  and  $2h \sim 200$  m (Fig.  
 329 S6). The most damaged fault-zone structures reach  $\Delta \sim 0.85$  (H. Li et al., 2007; Yang  
 330 & Zhu, 2010), which is close to the minimum value required by our model to show sig-  
 331 nificant slip complexity (Fig. 2a,b). For  $\Delta \sim 0.85$  and a reasonable fault-zone thick-  
 332 ness  $2h$  from 100 m to 1 km, the rupture length required to develop pulses and back-propagating  
 333 fronts must be larger than 2 to 20 km (Fig. 2a,b). It is likely then that the quasi-static  
 334 LVFZ effects described here do not operate during very small slow slip events. The prop-  
 335 erties of fault zones where RTRs are observed are harder to be resolved compared to crustal  
 336 faults due to the larger depths involved. Dimensions of fault zones in subduction envi-  
 337 ronments have been inferred from observations in exhumed subduction zones (Rowe et  
 338 al., 2013) but their elastic properties remain poorly constrained. Receiver functions sug-  
 339 gest that the  $v_p/v_s$  ratio may increase over  $\sim 75\%$  due to over-pressurization of fluids  
 340 within the several-km-thick low-velocity zone that surrounds regions where tremors are  
 341 generated (Audet & Schaeffer, 2018; Calvert et al., 2020).

#### 342 4.4 Potential model limitations

343 Further research is warranted to investigate whether the effects observed in our ide-  
 344 alized fault zone model remain after releasing some of the simplifying assumptions, in  
 345 particular the quasi-dynamic approximation and the 2D tabular LVFZ geometry.

346 Quasi-dynamic simulations in the absence of a LVFZ qualitatively agree with fully-  
 347 dynamic simulations under a conventional Dieterich-Ruina friction law (Thomas et al.,

2014). However, dynamic simulations that include a LVFZ produce a range of fault zone waves, including reflected, trapped and head waves (Huang & Ampuero, 2011; Huang et al., 2014), which can perturb the dynamic stress on the fault and interfere with the quasi-static mechanism highlighted in the present work. Preliminary results suggest that dynamic effects modulate, but do not obliterate the quasi-static effects reported here (Flores-Cuba et al., 2020). Similarly, in previous dynamic single-rupture simulations (Huang et al., 2014) dynamic LVFZ wave effects modulate, but do not obliterate the generation of pulses by another mechanism, enhanced velocity-weakening friction. An important open question is whether the dynamic effects of fault zone waves allow the slip complexity revealed here to operate over a broader range of LVFZ property values, including the lower, commonly observed levels of fault-zone damage.

The direction of slip is not important in the context of our quasi-dynamic model. Our anti-plane results can be transferred to in-plane slip by replacing  $\mu$  with  $\mu/(1-\nu)$ , where  $\nu$  is Poisson's ratio. However, in-plane dynamical models can promote additional slip complexity, for instance transitions to super-shear rupture speed which are relevant for the interpretation of past earthquakes (Huang et al., 2016; Oral et al., 2020).

The 3D structure of damage zones observed in the field is more complicated than a simple 2D tabular region, usually displaying flower structures with wider thickness at shallower depth (Finzi et al., 2009; Mitchell & Faulkner, 2009; Savage & Brodsky, 2011). Moreover, LVFZ properties are not uniform along strike as the fault-zone thickness varies with along-strike changes in fault geometry and the total amount of slip locally accumulated over time (Mitchell & Faulkner, 2009; C. Perrin et al., 2016; Ampuero & Mao, 2017). How such systematic variations of LVFZ properties affect the rupture features highlighted here warrants further study. We expect that the promotion by LVFZ of pulses and back-propagating fronts reported in our 2D simulations should also appear in 3D simulations, as the static transfer mechanism is approximately the same (similar to Eq. 4 with  $k$  replaced by the modulus of the wavenumber vector).

The quasi-static pulse-generation mechanism revealed here should persist in a LVFZ without the sharp elasticity contrasts of a simple tabular damage zone, in contrast to the dynamic mechanism of pulse-generation by reflected waves (Huang et al., 2014). In fact, the static stress transfer in a model with exponential decay of damage as a function of distance from the fault (Ampuero et al., 2002) has the same essential features as in our tabular model (Eq. 4), in particular the same asymptotic behaviors highlighted in Fig. 4.

## 5 Conclusions

Our analytical arguments and simulation results show that rupture pulses emerge and persist across multiple earthquake cycles via quasi-static effects in a fault surrounded by a highly-damaged fault zone, independently of the dynamic effects induced by fault-zone-reflected waves. We develop a formal analogy between a fault zone model and a nearest-neighbor (Burridge-Knopoff) model that explains the emergence of pulses. Nearest-neighbor models are known to produce pulses and, within a certain range of length scales, the stress transfer in a damaged fault zone is approximately nearest-neighbor. Our results suggest that the earthquake rise-time should be proportional to fault zone thickness divided by rupture speed in highly-damaged faults.

We also showed that fault-zone effects can produce complex slip patterns, including back-propagating fronts that re-rupture previously healed fault segments. Such back-propagating fronts have been most recently observed in large earthquakes. The back-propagating fronts in our slow-slip models with highly-damaged fault zones are also analogous to rapid tremor reversals observed in Cascadia and Japan.

Overall, quasi-static fault-zone effects provide a simple mechanism to promote and sustain earthquake complexity, and a mechanical link between structural fault properties and seismicity. Our results further motivate the quest for higher temporal and spatial resolution in earthquake source studies. The systematic exploration of model parameters contained in our results provide targets for laboratory experiments aimed at understanding the interactions between rupture propagation and heterogeneous media.

### Acknowledgments

This work was supported by the Southern California Earthquake Center (SCEC) and by the French government through the FAULTS\_R\_GEMS project (ANR-17-CE31-0008) and the UCAJEDI Investments in the Future project (ANR-15-IDEX-01) managed by the National Research Agency (ANR). SCEC is funded by NSF Cooperative Agreement EAR-1600087 and USGS Cooperative Agreement G17AC00047. This is SCEC Contribution No. 10084.

### Author contributions

Both authors contributed to the writing of the manuscript and the interpretation of the numerical results. B.I. developed the scaling argument, performed the numerical simulations, and prepared the figures. J.-P. A. designed the study, developed the expressions for the spectral kernel, the static crack numerical solutions and the asymptotic analysis connecting the BK and LVFZ models.

### Data availability

Data sharing not applicable to this article as no datasets were generated or analyzed during the current study.

### Code availability

The Quasi-DYNAMIC earthquake simulator (QDYN) (Luo et al., 2017) used to compute our numerical models of earthquake cycles is available at [github.com/ydluo/qdyn](https://github.com/ydluo/qdyn). QDYN is freely available for academic research purposes and licensed by GNU General Public License, version 3.

### References

- Aagaard, B. T., & Heaton, T. (2008). Constraining fault constitutive behavior with slip and stress heterogeneity. *Journal of Geophysical Research: Solid Earth*, *113*(B4).
- Ampuero, J. P., & Mao, X. (2017). Upper limit on damage zone thickness controlled by seismogenic depth. *Fault Zone Dynamic Processes: Evolution of Fault Properties During Seismic Rupture*, *227*, 243.
- Ampuero, J.-P., & Rubin, A. M. (2008). Earthquake nucleation on rate and state faults—aging and slip laws. *Journal of Geophysical Research: Solid Earth*, *113*(B1).
- Ampuero, J.-P., Vilotte, J.-P., & Sanchez-Sesma, F. (2002). Nucleation of rupture under slip dependent friction law: simple models of fault zone. *Journal of Geophysical Research: Solid Earth*, *107*(B12).
- Audet, P., & Schaeffer, A. J. (2018). Fluid pressure and shear zone development over the locked to slow slip region in cascadia. *Science advances*, *4*(3), eaar2982.
- Barbot, S. (2019). Slow-slip, slow earthquakes, period-two cycles, full and partial ruptures, and deterministic chaos in a single asperity fault. *Tectonophysics*,

- 768, 228171.
- 442 Ben-Zion, Y., Peng, Z., Okaya, D., Seeber, L., Armbruster, J. G., Ozer, N., . . . Ak-  
 443 tar, M. (2003). A shallow fault-zone structure illuminated by trapped waves  
 444 in the Karadere–Duzce branch of the North Anatolian Fault, western Turkey.  
 445 *Geophysical Journal International*, 152(3), 699–717.
- 446 Beroza, G. C., & Mikumo, T. (1996). Short slip duration in dynamic rupture in the  
 447 presence of heterogeneous fault properties. *Journal of Geophysical Research:*  
 448 *Solid Earth*, 101(B10), 22449–22460.
- 449 Beroza, G. C., & Spudich, P. (1988). Linearized inversion for fault rupture be-  
 450 havior: Application to the 1984 morgan hill, california, earthquake. *Journal of*  
 451 *Geophysical Research: Solid Earth*, 93(B6), 6275–6296.
- 452 Brener, E. A., Aldam, M., Barras, F., Molinari, J.-F., & Bouchbinder, E. (2018).  
 453 Unstable slip pulses and earthquake nucleation as a nonequilibrium first-order  
 454 phase transition. *Physical review letters*, 121(23), 234302.
- 455 Burridge, R., & Knopoff, L. (1967). Model and theoretical seismicity. *Bulletin of the*  
 456 *seismological society of america*, 57(3), 341–371.
- 457 Calvert, A. J., Bostock, M. G., Savard, G., & Unsworth, M. J. (2020). Cascadia low  
 458 frequency earthquakes at the base of an overpressured subduction shear zone.  
 459 *Nature Communications*, 11(1), 1–10.
- 460 Cattania, C. (2019). Complex earthquake sequences on simple faults. *Geophysical*  
 461 *Research Letters*.
- 462 Chester, F., & Logan, J. M. (1986). Implications for mechanical properties of brittle  
 463 faults from observations of the punchbowl fault zone, california. *Pure and ap-*  
 464 *plied geophysics*, 124(1-2), 79–106.
- 465 Cochard, A., & Madariaga, R. (1996). Complexity of seismicity due to highly rate-  
 466 dependent friction. *Journal of Geophysical Research: Solid Earth*, 101(B11),  
 467 25321–25336.
- 468 Cochard, A., & Rice, J. R. (1997). A spectral method for numerical elastodynamic  
 469 fracture analysis without spatial replication of the rupture event. *Journal of*  
 470 *the Mechanics and Physics of Solids*, 45(8), 1393–1418.
- 471 Cochran, E. S., Li, Y.-G., Shearer, P. M., Barbot, S., Fialko, Y., & Vidale, J. E.  
 472 (2009). Seismic and geodetic evidence for extensive, long-lived fault damage  
 473 zones. *Geology*, 37(4), 315–318.
- 474 Cruz-Atienza, V. M., Villafuerte, C., & Bhat, H. S. (2018). Rapid tremor migration  
 475 and pore-pressure waves in subduction zones. *Nature communications*, 9(1), 1–  
 476 13.
- 477 Day, S. M. (1982). Three-dimensional finite difference simulation of fault dynamics:  
 478 rectangular faults with fixed rupture velocity. *Bulletin of the Seismological So-*  
 479 *ciety of America*, 72(3), 705–727.
- 480 Day, S. M., Yu, G., & Wald, D. J. (1998). Dynamic stress changes during earth-  
 481 quake rupture. *Bulletin of the Seismological Society of America*, 88(2), 512–  
 482 522.
- 483 Dieterich, J. H. (1981). Constitutive properties of faults with simulated gouge. *Me-*  
 484 *chanical behavior of crustal rocks: the Handin volume*, 24, 103–120.
- 485 Erickson, B. A., Birnir, B., & Lavallée, D. (2011). Periodicity, chaos and localiza-  
 486 tion in a burridge–knopoff model of an earthquake with rate-and-state friction.  
 487 *Geophysical Journal International*, 187(1), 178–198.
- 488 Finzi, Y., Hearn, E. H., Ben-Zion, Y., & Lyakhovskiy, V. (2009). Structural proper-  
 489 ties and deformation patterns of evolving strike-slip faults: Numerical simula-  
 490 tions incorporating damage rheology. *Pure and Applied Geophysics*, 166(10-  
 491 11), 1537–1573.
- 492 Flores-Cuba, J. M., Ampuero, J.-P., Oral, E., & Idini, B. (2020). Fault damage  
 493 zones enhance earthquake rupture complexity over multiple cycles.
- 494 Gabriel, A.-A., Ampuero, J.-P., Dalguer, L. A., & Mai, P. M. (2012). The transition  
 495 of dynamic rupture styles in elastic media under velocity-weakening friction.
- 496



- 497 *Journal of Geophysical Research: Solid Earth*, 117(B9).
- 498 Harris, R. A., & Day, S. M. (1997). Effects of a low-velocity zone on a dynamic rup-  
499 ture. *Bulletin of the Seismological Society of America*, 87(5), 1267–1280.
- 500 Hawthorne, J., & Rubin, A. (2013b). Tidal modulation and back-propagating  
501 fronts in slow slip events simulated with a velocity-weakening to velocity-  
502 strengthening friction law. *Journal of Geophysical Research: Solid Earth*,  
503 118(3), 1216–1239.
- 504 Hawthorne, J., & Rubin, A. M. (2013a). Laterally propagating slow slip events  
505 in a rate and state friction model with a velocity-weakening to velocity-  
506 strengthening transition. *Journal of Geophysical Research: Solid Earth*,  
507 118(7), 3785–3808.
- 508 Heaton, T. H. (1990). Evidence for and implications of self-healing pulses of slip  
509 in earthquake rupture. *Physics of the Earth and Planetary Interiors*, 64(1), 1–  
510 20.
- 511 Hicks, S. P., Okuwaki, R., Steinberg, A., Rychert, C. A., Harmon, N., Abercrombie,  
512 R. E., ... others (2020). Back-propagating supershear rupture in the 2016 m  
513 w 7.1 romanche transform fault earthquake. *Nature Geoscience*, 1–7.
- 514 Horowitz, F. G., & Ruina, A. (1989). Slip patterns in a spatially homogeneous fault  
515 model. *Journal of Geophysical Research: Solid Earth*, 94(B8), 10279–10298.
- 516 Houston, H., Delbridge, B. G., Wech, A. G., & Creager, K. C. (2011). Rapid tremor  
517 reversals in Cascadia generated by a weakened plate interface. *Nature Geo-  
518 science*, 4(6), 404.
- 519 Huang, Y., & Ampuero, J.-P. (2011). Pulse-like ruptures induced by low-velocity  
520 fault zones. *Journal of Geophysical Research: Solid Earth*, 116(B12).
- 521 Huang, Y., Ampuero, J.-P., & Helmberger, D. V. (2014). Earthquake ruptures  
522 modulated by waves in damaged fault zones. *Journal of Geophysical Research:  
523 Solid Earth*, 119(4), 3133–3154.
- 524 Huang, Y., Ampuero, J.-P., & Helmberger, D. V. (2016). The potential for super-  
525 shear earthquakes in damaged fault zones—theory and observations. *Earth and  
526 Planetary Science Letters*, 433, 109–115.
- 527 Idini, B., & Ampuero, J.-P. (2017). Rupture complexity promoted by damaged fault  
528 zones in earthquake cycle models.
- 529 Johnson, E. (1990). On the initiation of unidirectional slip. *Geophysical Journal In-  
530 ternational*, 101(1), 125–132.
- 531 Kaneko, Y., Ampuero, J.-P., & Lapusta, N. (2011). Spectral-element simulations of  
532 long-term fault slip: Effect of low-rigidity layers on earthquake-cycle dynamics.  
533 *Journal of Geophysical Research: Solid Earth*, 116(B10).
- 534 Lewis, M., Peng, Z., Ben-Zion, Y., & Vernon, F. (2005). Shallow seismic trapping  
535 structure in the san jacinto fault zone near anza, california. *Geophysical Jour-  
536 nal International*, 162(3), 867–881.
- 537 Lewis, M. A., & Ben-Zion, Y. (2010). Diversity of fault zone damage and trapping  
538 structures in the Parkfield section of the San Andreas Fault from comprehen-  
539 sive analysis of near fault seismograms. *Geophysical Journal International*,  
540 183(3), 1579–1595.
- 541 Li, H., Zhu, L., & Yang, H. (2007). High-resolution structures of the Landers fault  
542 zone inferred from aftershock waveform data. *Geophysical Journal Interna-  
543 tional*, 171(3), 1295–1307.
- 544 Li, Y.-G., Chen, P., Cochran, E. S., Vidale, J. E., & Burdette, T. (2006). Seismic  
545 evidence for rock damage and healing on the san andreas fault associated with  
546 the 2004 m 6.0 parkfield earthquake. *Bulletin of the Seismological Society of  
547 America*, 96(4B), S349–S363.
- 548 Li, Y.-G., Leary, P., Aki, K., & Malin, P. (1990). Seismic trapped modes in the  
549 oroville and san andreas fault zones. *Science*, 249(4970), 763–766.
- 550 Li, Y.-G., Vidale, J. E., Day, S. M., & Oglesby, D. D. (2002). Study of the 1999 M  
551 7.1 Hector Mine, California, earthquake fault plane by trapped waves. *Bulletin*



- 552           of the *Seismological Society of America*, 92(4), 1318–1332.
- 553 Luo, Y., & Ampuero, J.-P. (2017). Tremor migration patterns and the collective be-  
554           havior of deep asperities mediated by creep.
- 555 Luo, Y., Ampuero, J.-P., Galvez, P., van den Ende, M., & Idini, B. (2017).  
556           *QDYN: a Quasi-DYNamic earthquake simulator (v1.1)*. Zenodo.  
557           (doi:10.5281/zenodo.322459)
- 558 Luo, Y., & Liu, Z. (2019). Rate-and-state model casts new insight into episodic  
559           tremor and slow-slip variability in cascadia. *Geophysical Research Letters*.
- 560 Meng, L., Ampuero, J., Page, M., & Hudnut, K. (2011). Seismological evidence and  
561           dynamic model of reverse rupture propagation during the 2010 m7. 2 el mayor  
562           cucapah earthquake. In *Agu fall meeting abstracts*.
- 563 Meng, L., Ampuero, J.-P., Stock, J., Duputel, Z., Luo, Y., & Tsai, V. (2012). Earth-  
564           quake in a maze: Compressional rupture branching during the 2012 mw 8.6  
565           sumatra earthquake. *Science*, 337(6095), 724–726.
- 566 Michel, S., Gualandi, A., & Avouac, J.-P. (2019). Similar scaling laws for earth-  
567           quakes and cascadia slow-slip events. *Nature*, 574(7779), 522–526.
- 568 Mitchell, T., & Faulkner, D. (2009). The nature and origin of off-fault damage  
569           surrounding strike-slip fault zones with a wide range of displacements: A field  
570           study from the Atacama fault system, northern Chile. *Journal of Structural*  
571           *Geology*, 31(8), 802–816.
- 572 Mizuno, T., Kuwahara, Y., Ito, H., & Nishigami, K. (2008). Spatial variations in  
573           fault-zone structure along the nojima fault, central japan, as inferred from  
574           borehole observations of fault-zone trapped waves. *Bulletin of the Seismological*  
575           *Society of America*, 98(2), 558–570.
- 576 Nedimović, M. R., Hyndman, R. D., Ramachandran, K., & Spence, G. D. (2003).  
577           Reflection signature of seismic and aseismic slip on the northern cascadia sub-  
578           duction interface. *Nature*, 424(6947), 416.
- 579 Nielsen, S., & Madariaga, R. (2003). On the self-healing fracture mode. *Bulletin of*  
580           *the Seismological Society of America*, 93(6), 2375–2388.
- 581 Noda, H., Dunham, E. M., & Rice, J. R. (2009). Earthquake ruptures with thermal  
582           weakening and the operation of major faults at low overall stress levels. *Jour-*  
583           *nal of Geophysical Research: Solid Earth*, 114(B7).
- 584 Oral, E., Weng, H., & Ampuero, J. P. (2020). Does a damaged-fault zone mit-  
585           igate the near-field impact of supershear earthquakes?—application to the  
586           2018 7.5 palu, indonesia, earthquake. *Geophysical Research Letters*, 47(1),  
587           e2019GL085649.
- 588 Peng, Z., Ben-Zion, Y., Michael, A. J., & Zhu, L. (2003). Quantitative analysis of  
589           seismic fault zone waves in the rupture zone of the 1992 landers, california,  
590           earthquake: evidence for a shallow trapping structure. *Geophysical Journal*  
591           *International*, 155(3), 1021–1041.
- 592 Perrin, C., Manighetti, I., Ampuero, J.-P., Cappa, F., & Gaudemer, Y. (2016). Lo-  
593           cation of largest earthquake slip and fast rupture controlled by along-strike  
594           change in fault structural maturity due to fault growth. *Journal of Geophysical*  
595           *Research: Solid Earth*, 121(5), 3666–3685.
- 596 Perrin, G., Rice, J. R., & Zheng, G. (1995). Self-healing slip pulse on a frictional  
597           surface. *Journal of the Mechanics and Physics of Solids*, 43(9), 1461–1495.
- 598 Rice, J. R. (1993). Spatio-temporal complexity of slip on a fault. *Journal of Geo-*  
599           *physical Research: Solid Earth*, 98(B6), 9885–9907.
- 600 Roland, E., Lizarralde, D., McGuire, J. J., & Collins, J. A. (2012). Seismic veloc-  
601           ity constraints on the material properties that control earthquake behavior  
602           at the quebrada-discovery-gofar transform faults, east pacific rise. *Journal of*  
603           *Geophysical Research: Solid Earth*, 117(B11).
- 604 Ross, Z. E., Idini, B., Jia, Z., Stephenson, O. L., Zhong, M., Wang, X., . . . others  
605           (2019). Hierarchical interlocked orthogonal faulting in the 2019 ridgecrest  
606           earthquake sequence. *Science*, 366(6463), 346–351.

- 607 Rowe, C. D., Moore, J. C., Remitti, F., & Scientists, I. E. T. (2013). The thickness  
608 of subduction plate boundary faults from the seafloor into the seismogenic  
609 zone. *Geology*, *41*(9), 991–994.
- 610 Rubin, A., & Ampuero, J.-P. (2005). Earthquake nucleation on (aging) rate and  
611 state faults. *J. Geophys. Res.-Sol. Ea.*, *110*(B11).
- 612 Ruina, A. (1980). Friction laws and instabilities: a quasi-static analysis of some dry  
613 friction behaviour. *Ph. D. thesis, Division of Engineering, Brown University*.
- 614 Ruina, A. (1983). Slip instability and state variable friction laws. *J. Geophys. Res.-*  
615 *Sol. Ea.*, *88*(B12), 10359–10370.
- 616 Savage, H. M., & Brodsky, E. E. (2011). Collateral damage: Evolution with dis-  
617 placement of fracture distribution and secondary fault strands in fault damage  
618 zones. *Journal of Geophysical Research: Solid Earth*, *116*(B3).
- 619 Thakur, P., Huang, Y., & Kaneko, Y. (2020). Effects of low-velocity fault damage  
620 zones on long-term earthquake behaviors on mature strike-slip faults. *Journal*  
621 *of Geophysical Research: Solid Earth*, e2020JB019587.
- 622 Thomas, M. Y., Lapusta, N., Noda, H., & Avouac, J.-P. (2014). Quasi-dynamic  
623 versus fully dynamic simulations of earthquakes and aseismic slip with and  
624 without enhanced coseismic weakening. *Journal of Geophysical Research: Solid*  
625 *Earth*, *119*(3), 1986–2004.
- 626 Uchide, T., Yao, H., & Shearer, P. M. (2013). Spatio-temporal distribution of  
627 fault slip and high-frequency radiation of the 2010 el mayor-cucapah, mexico  
628 earthquake. *Journal of Geophysical Research: Solid Earth*, *118*(4), 1546–1555.
- 629 Vallée, M., Grandin, R., Nocquet, J.-M., Villegas, J.-C., Vaca, S., Xie, Y., ... Jarrin,  
630 P. (2020). Rupture characteristics of the 2019 north peru intraslab earthquake  
631 (mw8. 0). In *Egu general assembly conference abstracts* (p. 10429).
- 632 Yang, H., & Zhu, L. (2010). Shallow low-velocity zone of the San Jacinto fault  
633 from local earthquake waveform modelling. *Geophysical Journal International*,  
634 *183*(1), 421–432.
- 635 Yang, H., Zhu, L., & Cochran, E. S. (2011). Seismic structures of the calico fault  
636 zone inferred from local earthquake travel time modelling. *Geophysical Journal*  
637 *International*, *186*(2), 760–770.